APPLIED ORGANOMETALLIC CHEMISTRY
Appl. Organometal. Chem. 2005; **19**: 658–671
Main Group Metal Compounds
Published online 4 March 2004 in Wiley InterScience (www.interscience.wiley.com). DOI:10.1002/aoc.722

Atmospheric pressure deposition of fluorine-doped SnO_2 thin films from organotin fluorocarboxylate precursors

Mary F. Mahon[1], Kieran C. Molloy[1]*, Joanne E. Stanley[1], David W. H. Rankin[2], Heather E. Robertson[2] and Blair F. Johnston[2]

[1]Department of Chemistry, University of Bath, Claverton Down, Bath BA2 7AY, UK
[2]School of Chemistry, University of Edinburgh, West Mains Road, Edinburgh EH9 3JJ, UK

Received 6 May 2004; Revised 10 June 2004; Accepted 11 June 2004

Nine organotin fluorocarboxylates $R_nSnO_2CR_f$ ($n = 3$, R = Bu, $R_f = CF_3$, C_2F_5, C_3F_7, C_7F_{15}; R = Et, $R_f = CF_3$, C_2F_5; R = Me, $R_f = C_2F_5$; n = 2, R = Me, $R_f = CF_3$) have been synthesized; key examples have been used to deposit fluorine-doped SnO_2 thin films by atmospheric pressure chemical vapour deposition. $Et_3SnO_2CC_2F_5$, in particular, gives high-quality films with fast deposition rates despite adopting a polymeric, carboxylate-bridged structure in the solid state, as determined by X-ray crystallography. Gas-phase electron diffraction on the model compound $Me_3SnO_2CC_2F_5$ shows that accessible conformations do not allow contact between tin and fluorine, and that direct transfer is therefore unlikely to be part of the mechanism for fluorine incorporation in SnO_2 films. The structure of $Me_2Sn(O_2CCF_3)_2(H_2O)$ has also been determined and adopts a *trans*-Me_2SnO_3 coordination sphere about tin in which each carboxylate group is monodentate. Copyright © 2005 John Wiley & Sons, Ltd.

KEYWORDS: tin oxide; CVD; fluorocarboxylate; X-ray structure; electron diffraction

INTRODUCTION

There have been numerous studies on deposition of doped SnO_2 thin films, including both Group 15 and Group 17 dopants. Among these, by far the most widely studied is fluerine-doped SnO_2, as this transparent conducting material has been commercially exploited in such diverse areas as liquid-crystal displays, electrochromic devices, and solar control coatings on glass. Thin films of this material have been deposited by a number of methods, including sol–gel, spray pyrolysis, and sputtering, but chemical vapour deposition (CVD) offers the most attractive route, particularly for producing uniform coating of large areas. Our previous paper in this journal issue cites the relevant references to all these topics.

Single-source precursors that lead directly to $F:SnO_2$ are far less common than routes that involve multiple sources, and, as far as we are aware, detailed reports have only involved $Sn(O_2CCF_3)_2$,[1] $Sn[OCH(CF_3)_2]_4(HNMe_2)_2$,[2] $Sn[OCH(CF_3)_2]_2{\cdot}L$ ($L = HNMe_2$, C_5H_5N),[2,3] and $Bu_2Sn(O_2CCF_3)_2$.[4] Our own interest in this problem has caused us to evaluate a series of organotin(IV) fluoroalkanes, fluoroalkoxides and fluorocarboxylates as possible single-source solutions,[5] and it is this latter compound class that is the focus of this report. The use of organotin fluorocarboxylates as CVD precursors, either alone[6] or as one component of a mixture,[7] has been reported by others, predominantly in the patent literature.[8–10] The chemistry of organotin fluorocarboxylates has also attracted interest due to their potential anti-tumour activity.[11]

*Correspondence to: Kieran C. Molloy, Department of Chemistry, University of Bath, Claverton Down, Bath BA2 7AY, UK.
E-mail: k.c.molloy@bath.ac.uk
Contract/grant sponsor: Pilkington plc.
Contract/grant sponsor: EPSRC;
Contract/grant number: GR/R17768.

EXPERIMENTAL

General

Infrared spectra (cm^{-1}) were recorded as Nujol mulls between NaCl plates using a Nicolet 510P FT-IR spectrophotometer, and elemental analyses were performed using an Carlo-Erba Strumentazione E.A. model 1106 microanalyser operating at 500 °C. ^1H and ^{13}C NMR spectra were recorded on a

Jeol JNM-GX270 FT spectrometer, and ^{19}F and ^{119}Sn NMR spectra were recorded on a Jeol JNM-EX400 FT machine, all using saturated $CDCl_3$ solutions unless indicated otherwise; chemical shifts are in parts per million with respect to either Me_4Si, Me_4Sn or $CFCl_3$; coupling constants are in hertz. Details of our Mössbauer spectrometer and related procedures are given elsewhere;[12] data are in millimetres per second. Thermogravimetric studies were performed using a Perkin Elmer TGA7 analyser; samples were loaded in air and then the temperature was increased under a flow of dry nitrogen gas.

Dry solvents were obtained by distillation under inert atmosphere from the following drying agents: sodium–benzophenone (toluene, diethyl ether, tetrahydrofuran), calcium hydride (CH_2Cl_2), sodium (hexane). Standard Schlenk techniques were used throughout. Starting materials were obtained commercially and used without further purification.

Chemical vapour deposition

Details of our apparatus are given elsewhere.[13,14] In all cases, the substrate used was 4 mm glass that was undercoated with a thin film of SiCO to act as a 'blocking layer' to prevent sodium diffusion into the fluorine-doped tin oxide film. Approximately 10 g of precursor was used in each series of experiments; details of the relevant deposition conditions are given in Table 1. All films adhered well to the glass and could not be removed easily without relatively harsh treatment.

Film analysis

The X-ray diffraction (XRD) equipment consisted of a Philips PW1130 generator operating at 45 kV and 40 mA to power a copper long fine-focus X-ray tube. A PW 1820 goniometer fitted with glancing-angle optics and proportional X-ray detector was used. The non-focusing thin film optics employed a 0.25° primary beam slit to irradiate the specimen at a fixed incident angle of 1.5°. Diffraction radiation from the sample was collimated with a flat-plate collimator and passed through a graphite flat crystal monochromator to isolate diffracted copper Kα peaks onto the detector. The equipment was situated in a total enclosure to provide radiation safety for the highly collimated narrow beams of X-rays. Data were acquired by a PW1710 microprocessor and processed using Philips APD VMS software. Crystalline phases were identified from the International Centre for Diffraction Data database. Samples of coating for XRD were of approximate dimensions 1.5 cm × 2.0 cm. Crystallite size was determined from line broadening using the Scherrer equation.[15] The instrumental effect was removed using the NIST SRM660 lanthanum hexaboride standard. These operating conditions were used in preference to conventional Bragg–Brentano optics for thin films to give an order of magnitude increase in count rate from a fixed volume of coating with little contribution from the substrate.

Film thickness was determined by etching a thin strip of the film with zinc powder and 50% HCl solution. This created a step in the film, which was measured with a Dektak stylus technique.

Haze was measured on a Pacific Scientific Hazeguard meter and with a barium fluoride detector. The calculation of haze was carried out by measurement of the specular light and diffusive light. Specular light is defined as light transmitted straight through the sample within ±2.5° of normal incidence and the diffusive light is defined as light scattered beyond 2.5°. The initial measurement was carried out with the specular detector slot closed and, therefore, a value for the sum of the specular light and the diffusive light was obtained. The specular light slot was then opened and a measurement of the diffusive light was obtained.[13]

Emissivity data (integral of total emittance between 5 and 50 μm divided by the integral from 5 to 50 μm of the total emittance of a blackbody at room temperature) were then calculated from the infrared reflectance spectra, measured using a two-beam Perkin Elmer 883 machine and measured against a rhodium mirror standard.[16]

Sheet resistance was measured with a four-point probe on an electrically isolated scribed circle of film ($\square = 25\ cm^2$) and corrected using a conversion factor, the value being dependent on the diameter of the scribed circle.

Fluorine was determined by X-ray fluorescence measurements, made on a Philips PW1400 machine fitted with a scandium target X-ray tube. The penetration depth achieved was between 9 and 10 μm, so the result obtained was throughout the thickness of the coating. The analysis was performed on approximately 6 cm^2 of material.

Table 1. Conditions for the atmospheric pressure CVD of fluorine-doped SnO_2 using fluorinated organotin carboxylate precursors

	1	2	3	6	7
Reactor temperature (°C)	564	564	570	541	560
Bubbler temperature (°C)	110	125	116	150	165
Heater tapes (°C)	200	200	200	200	250
Diluent flow (l min^{-1})	3.00	3.00	3.00	2.75	2.75
Carrier flow (l min^{-1})	1.0	1.0	1.0	1.0	1.0
Oxygen flow (l min^{-1})	0.6	0.6	0.6	0.6	0.6
Run time (min)	25	25	20	3	1.5

Synthesis

*Preparation of tributyltin trifluoroacetate, $Bu_3SnO_2CCF_3$ (**1**)*

Sodium trifluoroacetate (5.06 g, 37 mmol) in ethanol (100 ml) was added to a solution of tributyltin chloride (12.08 g,

37 mmol) in ethanol (75 ml). The mixture was refluxed for 2 h before removing the solvent *in vacuo* to yield a white solid. This was recrystallized from 40°–60° petroleum ether to yield white needles. The product was then dried under vacuum to give tributyltin trifluoroacetate (8.69 g, 58%, m.p. 49–52 °C). Anal. Found (calc. for $C_{14}H_{27}F_3O_2Sn$): C, 41.8 (41.7)%; H, 6.99 (6.77)%. Mössbauer: IS = 1.51 mm s^{-1}; QS = 4.06 mm s^{-1} (lit: IS = 1.62 mm s^{-1}, QS = 4.40 mm s^{-1}).[17] ^{119}Sn NMR: 172.3. ^{1}H NMR: 0.92 [9H, t, CH_3(CH$_2$)$_3$], $^3J(^1H–^1H)$ = 7 Hz; 1.38 [12H, m, C_4H_9]; 1.64 [6H, m, C_4H_9]. ^{13}C NMR: 13.5 [$CH_3(CH_2)_3$]; 17.3 [$CH_3(CH_2)_2CH_2$]; 26.9 [$CH_3CH_2(CH_2)_2$]; 27.5 [$CH_3CH_2CH_2CH_2$]. $^1J(^{13}C–^{119}Sn)$ = 334 Hz. C–F carbon not observed. IR (cm^{-1}): 1721, 1678 [$\nu_a(CO_2)$], 1586, 1447 [$\nu_s(CO_2)$], 1206, 1160, 849, 793, 700, 675, 604.

*Preparation of tributyltin pentafluoropropionate, $Bu_3SnO_2CC_2F_5$ (**2**)*

The synthetic method described above for **1** was repeated using sodium pentafluoropropionate (6.16 g, 35 mmol) and tributyltin chloride (11.26 g, 35 mmol). White needles of tributyltin pentafluoropropionate (9.07 g, 60%, m.p. 64–66 °C) were obtained. Anal. Found (calc. for $C_{15}H_{27}F_5O_2Sn$): C, 40.0 (39.8)%; H, 6.35 (6.02)%. Mössbauer: IS = 1.52; QS = 4.12. ^{119}Sn NMR: 174.5. ^{1}H NMR: 0.92 [9H, t, CH_3(CH$_2$)$_3$], $^3J(^1H–^1H)$ = 7 Hz; 1.37 [12H, m, C_4H_9]; 1.64 [6H, m, C_4H_9]. ^{13}C NMR: 13.6 [$CH_3(CH_2)_3$]; 17.4 [$CH_3(CH_2)_2CH_2$]; 26.9 [$CH_3CH_2(CH_2)_2$]; 27.5 [$CH_3CH_2CH_2CH_2$]. $^1J(^{13}C–^{119}Sn)$ = 332 Hz. C–F carbon atoms not observed. IR (cm^{-1}): 1678 [$\nu_a(CO_2)$], 1424 [$\nu_s(CO_2)$], 1329, 1292, 1221, 1169, 1078, 1034, 963, 880, 824, 702, 675.

*Preparation of tributyltin heptafluorobutyrate, $Bu_3SnO_2CC_3F_7$ (**3**)*

Sodium heptafluorobutyrate (9.38 g, 40 mmol) and tributyltin chloride (12.95 g, 40 mmol) were used in the methodology described for **1** to produce crystals of tributyltin heptafluorobutyrate (11.00 g, 55%, m.p. 58 °C) (lit: 62–64 °C).[18] Anal. Found (calc. for $C_{16}H_{27}F_7O_2Sn$): C, 38.2 (38.2)%; H, 5.59 (5.42)%. Mössbauer: IS = 1.52; QS = 4.05. ^{119}Sn NMR: 175.1. ^{1}H NMR: 0.92 [9H, t, CH_3(CH$_2$)$_3$], $^3J(^1H–^1H)$ = 7 Hz; 1.36 [12H, m, C_4H_9]; 1.65 [6H, m, C_4H_9]. ^{13}C NMR: 13.5 [$CH_3(CH_2)_3$]; 17.4 [$CH_3(CH_2)_2CH_2$]; 26.9 [$CH_3CH_2(CH_2)_2$]; 27.4 [$CH_3CH_2CH_2CH_2$]. $^1J(^{13}C–^{119}Sn)$ = 336 Hz. C–F carbon atoms not observed. IR (cm^{-1}): 1678 [$\nu_a(CO_2)$], 1418 [$\nu_s(CO_2)$], 1275, 1190, 1086, 968, 934, 816, 673.

*Preparation of tributyltin pentadecafluorooctanoate, $Bu_3SnO_2CC_7F_{15}$ (**4**)*

Penta-decafluorooctanoic acid (1.77 g, 4 mmol) in toluene (100 ml) was added to bis(tributyltin) oxide (1.19 g, 2 mmol) and the mixture refluxed for 2 h. The water formed was azeotropically removed using a Dean and Stark apparatus. The solvent was removed *in vacuo* to leave the title compound as an oily semi-solid material (1.02 g, 36%) (lit. m.p. 45–47 °C).[18] Analysis: found (calc. for $C_{20}H_{27}F_{15}O_2Sn$): C 33.9 (34.2)%; H 3.88 (3.87)%. Mössbauer: IS = 1.53; QS = 4.07. ^{119}Sn NMR: 167.2. ^{1}H NMR: 0.92 [9H, t, CH_3(CH$_2$)$_3$], $^3J(^1H–^1H)$ = 7 Hz; 1.38 [12H, m, C_4H_9]; 1.65 [6H, m, C_4H_9]. ^{13}C NMR: 13.4 [$CH_3(CH_2)_3$]; 17.5 [$CH_3(CH_2)_2CH_2$]; 26.9 [$CH_3CH_2(CH_2)_2$]; 27.5 [$CH_3CH_2CH_2CH_2$]. $^1J(^{13}C–^{119}Sn)$ = 343 Hz. C–F carbon atoms not observed. IR (cm^{-1}): 1688 [$\nu_a(CO_2)$], 1466 [$\nu_s(CO_2)$], 1362, 1242, 1140, 1106, 1020, 667.

*Preparation of triethyltin trifluoroacetate, $Et_3SnO_2CCF_3$ (**5**)*

The method previously used to synthesize **1** was utilized. Sodium trifluoroacetate (1.36 g, 10 mmol) and triethyltin chloride (2.41 g, 10 mmol) were reacted to produce white crystals of triethyltin trifluoroacetate (0.72 g, 23%, m.p. 119 °C) (lit: 120–121 °C).[19] Analysis: found (calc. for $C_8H_{15}F_3O_2Sn$): C 30.2 (30.1)%; H 4.82 (4.75)%. Mössbauer: IS = 1.53; QS = 4.17. ^{119}Sn NMR: 164.7. ^{1}H NMR: 1.34 [15H, m, C_2H_5]. ^{13}C NMR: 8.88 [CH_3CH_2]; 9.54 [CH_3CH_2]. $^1J(^{13}C–^{119}Sn)$ = 322 Hz. C–F carbon not observed. IR (cm^{-1}): 1680, 1653 [$\nu_a(CO_2)$], 1590, 1456 [$\nu_s(CO_2)$], 1196, 1150, 1019, 959, 851, 795, 679.

*Preparation of triethyltin pentafluoropropionate, $Et_3SnO_2CC_2F_5$ (**6**)*

Sodium pentafluoropropionate (10.26 g, 55 mmol) and triethyltin chloride (13.36 g, 55 mmol) were used in the methodology described for **1** to form triethyltin pentafluoropropionate (9.08 g, 45%, m.p. 94 °C) as a crystalline material. Anal. Found (calc. for $C_9H_{15}F_5O_2Sn$): C, 29.3 (29.3)%; H, 4.12 (4.10)%. Mössbauer: IS = 1.54; QS = 4.12. ^{119}Sn: 160.5. ^{1}H NMR: 1.33 [15H, m, C_2H_5]. ^{13}C NMR: 8.89 [CH_3CH_2]; 9.45 [CH_3CH_2]. $^1J(^{13}C–^{119}Sn)$ = 326 Hz. C–F carbon atoms not observed. IR (cm^{-1}): 1659 [$\nu_a(CO_2)$], 1462 [$\nu_s(CO_2)$], 1426, 1335, 1219, 1171, 1038, 1017, 957, 826, 677.

*Preparation of dimethyltin bis-(trifluoroacetate), $Me_2Sn(O_2CCF_3)_2$ (**7**)*

1 M sodium hydroxide was added to dimethyltin dichloride (25.00 g, 110 mmol) in distilled water (100 ml) until pH 9 was achieved, quantitatively precipitating dimethyltin oxide. The oxide was collected by filtration, washed several times with distilled water, then dried in an oven overnight. Dimethyltin oxide (6.00 g, 36 mmol) and a large excess of trifluoroacetic anhydride (20.00 ml, 140 mmol) were refluxed for 3 h, then the excess anhydride was distilled off under a nitrogen atmosphere to leave a white solid. This solid was subsequently sublimed under reduced pressure to yield the product as a white crystalline material (11.10 g, 82%, sublimation temp. 80 °C/1.5 mmHg, m.p. 140 °C). Anal. found (calc. for $C_6H_6F_6O_4Sn$): C, 19.1 (19.2)%; H, 1.63 (1.62)%. Mössbauer: IS = 1.47 mm s^{-1}; QS = 4.36 mm s^{-1}.

*Preparation of dimethyltin bis-(trifluoroacetate) monohydrate, $Me_2Sn(O_2CCF_3)_2(OH_2)$ (**8**)*

Compound **8** was obtained following recrystallization of **7** from chloroform in air, m.p. 220 °C. Anal. Found (calc. for $C_6H_8F_6O_5Sn$): C, 18.3 (18.3)%; H, 2.07 (2.06)%. Mössbauer: IS = 1.30; QS = 3.85. ^{119}Sn NMR: −139.4; −138.6.

^{1}H NMR: 1.25 [s, $(CH_3)_2Sn$]; $^2J(^1H-^{119}Sn) = 81$ Hz. ^{13}C NMR: 5.8 [$(CH_3)_2Sn$]; $^1J(^{13}C-^{119}Sn) = 702$ Hz; 116.5 [$Sn(O_2CCF_3)_2$]; 163.0 [$Sn(O_2CCF_3)_2$]. ^{19}F NMR: −75.6 [$Sn(O_2CCF_3)_2$]. IR (cm^{-1}): 3386, 1671 [$\nu_a(CO_2)$], 1453 [$\nu_s(CO_2)$], 1202, 1146, 855, 789.

*Preparation of trimethyltin pentafluoropropionate, $Me_3SnO_2CC_2F_5$ (**9**)*

The synthetic method described above for **1** was repeated using sodium pentafluoropropionate (4.66 g, 25 mmol) and trimethyltin chloride (5.00 g, 25 mmol). White needles of trimethyltin pentafluoropropionate (6.20 g, 76%) were obtained from petroleum ether (m.p. 110–113 °C). Anal. Found (calc. for $C_6H_9F_5O_2Sn$): C, 22.0 (22.0)%; H, 2.78 (2.78)%. ^{119}Sn NMR: 190.7. ^{1}H NMR: 0.64 [9H, s, CH_3]. ^{13}C NMR: −2.54 [CH_3]; $^1J(^{13}C-^{119,117}Sn) = 431$, 411; $^2J(^1H-^{117,119}Sn) = 56$, 59 Hz.

Crystallography

Crystallographic details for **6** and **8** are given in Table 2. Crystallographic quality crystals of $Et_3SnO_2CC_2F_5$ (**6**) were obtained by slow evaporation of a saturated solution in 40°–60° petroleum ether at room temperature. The crystals were stable to light and to atmosphere, but data collection had to be carried out at 170 K owing to the decay of the compound in the X-ray beam at room temperature. Suitable crystals of $Me_2Sn(O_2CCF_3)_2(OH_2)$ (**8**), were obtained by slow vacuum sublimation onto a cold finger. The crystals were found to be sensitive to air and moisture, and data collection was carried out at 170 K.

In both cases, data were collected on a CAD4 automatic four-circle diffractometer and Lorentz and polarization corrections were applied; for **6**, a correction was also made for absorption and crystal decay. All non-hydrogen atoms were treated anisotropically. Hydrogen atoms were included at calculated positions, except for the water hydrogen atoms [H(1A), H(1B)] in **8**, which were located and refined at a fixed distance of 98 pm from the parent atom O(5). Refinement was based on F^2.

Software used: SHELXS 86,[20] SHELX 93,[21] ORTEX,[22] DIFABS.[23]

Table 2. X-ray crystallographic data for **6** and **8**

	6	**8**
Empirical formula	$C_9H_{15}F_5O_2Sn$	$C_6H_8F_6O_5Sn$
Formula weight	368.90	392.81
Crystal system	Monoclinic	Monoclinic
Space group	$P2_1/c$	$P2_1/n$
a (pm)	805.7(1)	1083.3(1)
b (pm)	1040.6(2)	1143.6(2)
c (pm)	1625.4(3)	1089.3(2)
β (°)	99.65(1)	107.81(1)
Volume ($\times 10^6$ pm)	1343.5(4)	1284.8(3)
Z	4	4
μ(Mo Kα) (mm^{-1})	1.949	2.072
θ range (°)	2.3–23.9	2.3–22.9
Independent reflections	2100 ($R_{int} = 0.0650$)	1777 ($R_{int} = 0.0259$)
Final R_1, wR_2 ($I > 2\sigma(I)$)	0.037, 0.092	0.023, 0.056
Final R_1, wR_2 (all data)	0.066, 0.099	0.031, 0.061
CCDC number	228 004	228 905

Theoretical methods

Calculations were performed on a DEC Alpha APX 1000A workstation using the GAUSSIAN 94 program.[24] An extensive search of the potential energy surface of $Me_3SnO_2CC_2F_5$ (**9**) was undertaken at the HF/3–21G* level in order to locate all structurally stable conformers. Two conformers for **9** were found; the lower energy conformer had C_s symmetry and the higher energy one was found to have C_1 symmetry (Fig. 1). Further geometry optimizations were then undertaken for both minima with the D95 basis set[25] [a full double zeta basis set, including tin (Dunning THJ, unpublished results; 15s, 11p, 7d/11s, 7p, 4d)] at the HF level. The subsequent two sets of calculations used the

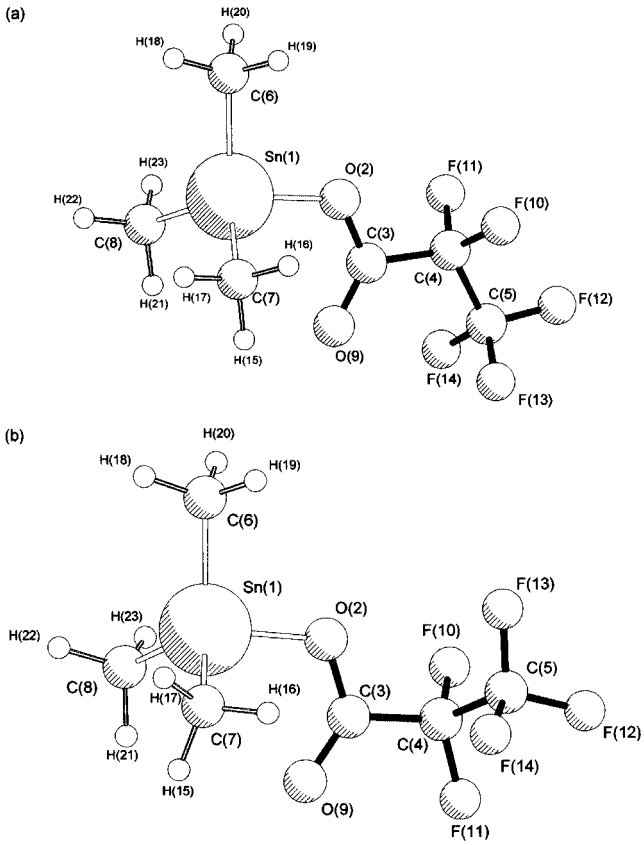

Figure 1. Structures determined *ab initio* for $Me_3SnO_2CC_2F_5$ (**9**) showing the atom numbering scheme: (a) the lowest energy conformer (1); (b) the conformer higher in energy by 1.2 kJ mol^{-1}.

LanL2DZ[26–28] effective core potential basis set (incorporating relativistic effects) for tin and D95 for the remaining atoms, at the HF and MP2 levels of theory. Vibrational frequencies were calculated from analytic second derivatives up to the D95 (fluorine, carbon, hydrogen, oxygen), LanL2DZ (tin)/HF level to confirm both conformers as local minima on the potential energy surface. The force constants obtained from these calculations were subsequently used to construct harmonic force fields for both conformers using the ASYM40 program,[29] modified to work for molecules with more than 40 atoms. As no fully assigned vibrational spectra are available for the compound to scale the force fields, a scaling factor of 0.9 was adopted for bond stretches, angle bends and torsions.[30] The scaled harmonic force fields were then used to provide estimates of amplitudes of vibration *u* for use in the gas-phase electron diffraction (GED) refinements. The results of these theoretical calculations are in Table 3, and results for all levels are in the supplementary data Table S1.

Gas-phase electron diffraction

GED scattering patterns were recorded for $Me_3SnO_2CC_2F_5$ (**9**) using the Edinburgh gas diffraction apparatus[31] with an accelerating voltage of *ca* 40 kV (electron wavelength *ca* 6.0 pm). Sample and nozzle temperatures were ~400 K and ~450 K respectively. Scattering intensities were recorded at nozzle-to-plate distances of 95.47 and 197.83 mm on Kodak Electron Image plates. The weighting points for the off-diagonal weight matrices, correlation parameters and scale factors for the two camera distances are given in Table 4, together with electron wavelengths, which were determined from the scattering patterns of benzene vapour recorded immediately after the patterns of $Me_3SnO_2CC_2F_5$ and analysed in exactly the same way, to minimize systematic errors in wavelengths and camera distances. A PDS densitometer at the Institute of Astronomy in Cambridge was used to convert the intensity patterns into digital form. Data reduction and least-squares refinements were carried out using the new 'ed@ed' program,[32] employing the scattering factors of Ross *et al.*[33]

Based on the *ab initio* molecular orbital (MO) calculations, a theoretical model containing two conformers, one with C_s and the other C_1 symmetry, was written for $Me_3SnO_2CC_2F_5$. To model the compound in the desired symmetries, 28 parameters were required. These consisted of eight bonded distance parameters (seven bond lengths and one difference parameter), 19 angles and one parameter to control the amount of conformer 1 in the two-conformer mixture. The starting values of these parameters for the r_a refinements were taken from the geometries optimized at the MP2 level. All 28 geometrical parameters and 11 groups of amplitudes of vibration were refined. Flexible restraints were employed during the refinement using the SARACEN method.[34,35] Altogether, 15 geometric and 10 amplitude restraints were employed.

Table 3. Calculated geometrical parameters for $Me_3SnO_2CC_2F_5$ (**9**) (distances in picometres, angles in degrees) from the *ab initio* MO theory study

	MP2/LanL2DZ (Sn) − D95	
	Conformer 1	Conformer 2
Bond distances		
Sn(1)–C(6)	212.7	212.7
Sn(1)–C(8)	212.6	212.5
Sn(1)–C(7)	212.6	212.6
C(3)–C(4)	154.3	154.5
C(4)–C(5)	154.5	154.7
C(4)–F(11)	136.2	136.3
C(4)–F(10)	136.2	135.3
C(5)–F(12)	134.6	134.2
C(5)–F(13)	134.1	133.9
C(5)–F(14)	134.1	135.0
Sn(1)–O(2)	205.2	205.0
C(3)–O(2)	131.4	131.6
C(3)═O(9)	123.3	122.9
Bond angles		
C(4)–C(5)–F(12)	109.4	110.5
C(4)–C(5)–F(13)	110.7	111.7
C(4)–C(5)–F(14)	110.7	109.0
F(10)–C(4)–F(11)	108.2	108.4
C(3)–C(4)–C(5)	114.5	112.8
O(2)–C(3)–C(4)	111.5	111.6
O(9)═C(3)–C(4)	122.0	121.6
C(6)–Sn(1)–O(2)	98.2	98.1
C(6)–Sn(1)–C(7)	114.2	114.4
C(7)–Sn(1)–C(8)	116.7	116.8
C(6)–Sn(1)–C(8)	114.2	113.9
C(8)–Sn(1)–O(2)	105.5	105.6
C(7)–Sn(1)–O(2)	105.5	105.4
Sn(1)–O(2)–C(3)	114.0	114.4
Sn(1)–C(7)–H(15)	110.5	110.6
Dihedral angles		
C(6)–Sn(1)–O(2)–C(3)	180.0	178.6
Sn(1)–O(2)–C(3)–C(4)	180.0	179.0
O(2)–C(3)–C(4)–C(5)	180.0	63.2
C(3)–C(4)–C(5)–F(12)	180.0	168.2

RESULTS AND DISCUSSION

Synthesis and spectroscopy

A series of fluorinated organotin carboxylates $R_nSn(O_2CR_f)_{4-n}$ has been prepared with a variation in both R and R_f, which has enabled the effects of both constituents in the CVD process to be explored. The majority of compounds synthesized were triorganotin derivatives, which were usually obtained via the conventional reaction of the triorganotin chloride and the sodium salt of the appropriate fluorinated carboxylic

Table 4. Nozzle-to-plate distances, weighting functions, correlation parameters, scale factors and electron wavelengths used in the electron-diffraction study

Nozzle-to-plate distance[a] (mm)	95.47	197.83
Δs (nm^{-1})	4	2
s_{min} (nm^{-1})	192	32
s_{w1} (nm^{-1})	212	52
s_{w2} (nm^{-1})	256	172
s_{max} (nm^{-1})	300	204
Correlation parameter	−0.2517	−0.0617
Scale factor[b]	1.545(97)	0.747(14)
Electron wavelength (pm)	6.016	6.016

[a] Determined by reference to the scattering pattern of benzene vapour.
[b] Values in parentheses are the estimated standard deviations.

acid.

$$R_3SnCl + NaO_2CR_f \xrightarrow{EtOH} R_3SnO_2CR_f + NaCl$$

R = Bu, $R_f = CF_3$ (**1**), C_2F_5 (**2**), C_3F_7 (**3**)

R = Et, $R_f = CF_3$ (**5**), C_2F_5 (**6**)

R = Me, $R_f = C_2F_5$ (**9**)

Recrystallization from 40°–60° petroleum ether yielded the compounds as colourless needles of high purity and in yields of 23–60%, with tributyltin derivatives being recovered in the higher quantities.

Compound **4** was prepared by the alternative route of reacting bis(tributyltin) oxide with the fluorinated carboxylic acid; the water generated was removed by a Dean and Stark separator.

$$(Bu_3Sn)_2O + 2C_7F_{15}CO_2H \xrightarrow[-H_2O]{\text{toluene}} 2Bu_3SnO_2CC_7F_{15} + H_2O \quad (\mathbf{4})$$

To explore the effect of an additional fluorinated group in the precursor, one diorganotin carboxylate was also prepared.

$$Me_2SnO + (CF_3CO)_2O \xrightarrow{\text{no solvent}} Me_2Sn(O_2CCF_3)_2 \quad (\mathbf{7})$$

Compound **7** was obtained as a pure white solid by sublimation. Crystallization from chloroform in air yielded the monohydrate $Me_2Sn(O_2CCF_3)_2 \cdot H_2O$ (**8**).

The tributyltin compounds were either oils (**4**) or low-melting-point solids (**1**: 49–52 °C; **2**: 64–66 °C; **3**: 58 °C). The melting points increased for the triethyl- (**5**: 119 °C; **6**: 94 °C), trimethyl- (**9**: 113 °C) and dimethyltin compounds (**7**: 140 °C; **8**: 220 °C). The melting point of **1** has been reported by others[36] as 255–260 °C, which we feel must be erroneous given the volatility of the compound.

In their infrared spectra, the difference in stretching frequency $\Delta\nu$ for $\nu_{asym}(CO_2)$ and $\nu_{sym}(CO_2)$, which lies in the range 197–254 cm^{-1}, indicates a bidentate bonding mode for the carboxylate in all the anhydrous compounds **1**–**7**. The Mössbauer QS values for the $R_3SnO_2CR_f$ compounds lie in the range 4.05–4.17 mm s^{-1}, indicating consistent *trans*-O_2SnC_3 geometry about tin, which is common to many triorganotin carboxylates;[37] data for **9** are consistent with these results.[17] The two diorganotin compounds have different spectra. Data for anhydrous **7** (4.36 mm s^{-1}) are typical of a six-coordinate *trans*-C_2SnO_4 geometry, as seen in the structure of the related compound $Me_2Sn(O_2CCH_3)_2$.[37] In contrast, QS data for hydrated **8** are noticeably reduced (3.85 mm s^{-1}), and crystallography identifies a change to a five-coordinated tin, incorporating monodentate carboxylate groups. $\Delta\nu$ for **8** (218 cm^{-1}) is somewhat misleading in this respect, but arises as a result of the extensive hydrogen bonding in which each C═O group is involved (*see* Crystallography section).

The NMR spectra of **1**–**6** and **9** are unexceptional. The ^1H and ^{13}C data confirm the integrity of the compounds, while $^1J(^{13}C–^{119}Sn)$ (322–343 Hz) and $\delta(^{119}Sn)$ (160.5–190.7 ppm) all indicate a four-coordinate tin atom in solution.[38] We have been unable to obtain reliable spectroscopic data for **7** in solution, due to the ease with which it becomes hydrated. However, for **8**, $^2J(^1H–^{119}Sn)$ of 81 Hz correlates with a calculated[39] C–Sn–C angle of 132.1° (140.1° found in the solid state), while the low frequency shifts for $\delta(^{119}Sn)$ (−139.4, −138.6 ppm) are all consistent with a coordination number CN > 4 for this species, even in solution.[38]

Crystallography

The structure of **6** is shown in Fig. 2 and confirms the inferences made from the spectral data. The polymeric nature and *trans*-O_2SnC_3 coordination sphere is common for R_3SnO_2CR'.[39] The nature of the bridging is anisotropic, in which tin forms one short [Sn(1)–O(1) 221.8(4) pm] and one relatively long [Sn(1)–O(2′) 248.1(4) pm; symmetry operation $1-x, \frac{1}{2}+y, \frac{1}{2}-z$] bond to oxygen. These bond lengths are comparable to other Sn–O bonds found in typical polymeric triorganotin carboxylates, with short (212.0–224.6 pm) and long (224–265 pm) bonds respectively. The O(1)–Sn(1)–O(2) angle [174.93(14)°] is also comparable to other angles found in typical polymeric triorganotin carboxylates (168.6–178.7°).[40]

The molecular structure of **8** is shown in Fig. 3 and the unit cell contents are shown in Fig. 4. The local geometry at tin is five-coordinate *cis*-$Me_2Sn(O_2CCF_3)_2(H_2O)$ (i.e. *cis*- methyl groups) and each carboxylate is bonded in a unidentate manner to the metal; water is coordinated directly to tin in an equatorial site. This contrasts with the polymeric structure adopted by the anhydrous compound, in which tin is in a six-coordinated environment.[41]

The unidentate nature of the carboxylate groups is evident by the short C═O [C(1)–O(2) 121.9(5) pm; C(3)–O(4) 121.4(5) pm] and long C–O [C(1)–O(1) 127.1(5) pm; C(3)–O(3) 128.0(5) pm] bonds, while the Sn(1)–O(5)

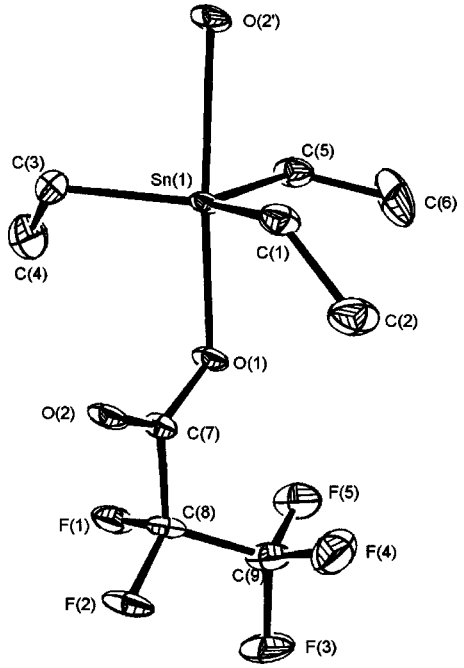

Figure 2. The polymeric structure of **6**, showing the labelling scheme used; thermal ellipsoids are at the 30% probability level and hydrogen atoms have been omitted for clarity. Selected geometric data: Sn(1)–C(1) 211.9(6), Sn(1)–C(3) 213.7(7), Sn(1)–C(5) 211.9(6), Sn(1)–O(1) 221.8(4), Sn(1)–O(2′) 248.1(4), O(1)–C(7) 128.4(7), O(2)–C(7) 122.4(7) pm; C(1)–Sn(1)–C(3) 127.0(3), C(1)–Sn(1)–C(5) 117.1(3), C(1)–Sn(1)–O(1) 96.0(2), C(1)–Sn(1)–O(2′) 85.4(2), C(3)–Sn(1)–C(5) 114.7(3), C(3)–Sn(1)–O(1) 95.1(2), C(3)–Sn(1)–O(2′) 87.9(2), C(5)–Sn(1)–O(1) 89.5(2), C(5)–Sn(1)–O(2′) 85.6(2), O(1)–Sn(1)–O(2′) 174.93(14)°; symmetry operation $1-x, \frac{1}{2}+y, \frac{1}{2}-z$.

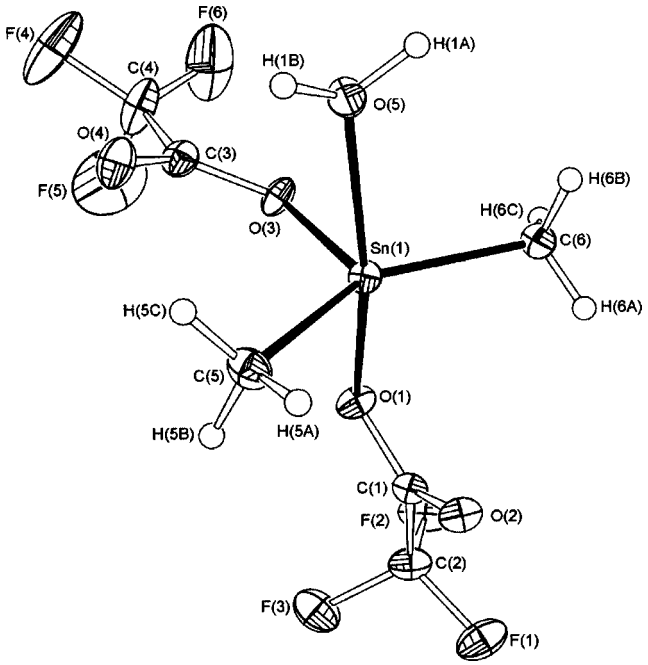

Figure 3. The structure of **8**, showing the labelling scheme used; thermal ellipsoids are at the 30% probability level. Selected geometric data: Sn(1)–C(5) 210.2(4), Sn(1)–C(6) 209.8(4), Sn(1)–O(1) 220.5(3), Sn(1)–O(3) 208.2(3), Sn(1)–O(5) 223.8(3), C(1)–O(1) 1.271(5), C(1)–O(2) 121.9(5), C(3)–O(3) 128.0(5), C(3)–O(4) 121.4(5) pm; C(5)–Sn(1)–C(6) 140.1(2), C(5)–Sn(1)–O(1) 96.71(14), C(5)–Sn(1)–O(3) 113.7(2), C(5)–Sn(1)–O(5) 91.45(14), C(6)–Sn(1)–O(1) 93.86(14), C(6)–Sn(1)–O(3) 106.12(14), C(6)–Sn(1)–O(5) 89.80(14), O(1)–Sn(1)–O(3) 79.15(11), O(1)–Sn(1)–O(5) 162.35(11), O(3)–Sn(1)–O(5) 83.24(11)°.

bond to water [223.8(3) pm] is the longest of the three Sn–O interactions [Sn(1)–O(1) 220.5(3) pm, Sn(1)–O(3) 208.2(3) pm]. The C(5)–Sn(1)–C(6) angle [140.1(2)°] represents a large deviation from an ideal angle of 120°.

Both hydrogen atoms of the coordinated water and the two carbonyl groups involve themselves in hydrogen bonding. H(1B) and O(4) link pairs of molecules into centrosymmetric dimers [O(4)–H(1B): 179(3) pm; <O(4)–H(1B)–O(5): 165(5)°]. These dimers are further linked into two-dimensional sheets by hydrogen bonds between H(1A) and <O(2′) [O(2′)–H(1A): 174(3) pm; O(5)–H(1A)–O(2′): 171(6)°; symmetry operation $\frac{1}{2}-x, y-\frac{1}{2}, \frac{1}{2}-z$].

It appears that three other structures of diorganotin dicarboxylates that contain a coordinated water molecule, namely $Bu_2Sn(O_2CCH_2C_6H_5)_2(H_2O)$,[42] $Cy_2Sn(O_2CCH_3)_2(H_2O)$[43] and a diorganotin derivative of a germatrane-substituted propanoic acid,[44] have been reported. However, all three structures are very different and consist of a seven-coordinate tin atom with *trans*-C_2SnO_5 pentagonal bipyramidal geometry resulting from the presence of two bidentate, chelating carboxylate groups. The structure of **8** is both unique and important, as it completes a sequence of structures that can be used to depict the reaction pathway by which diorganotin carboxylates are hydrolysed to the corresponding dimeric distannoxanes, $\{[R_2Sn(O_2CR')]_2O\}_2$ (Scheme 1).[45] The six-coordinated $R_2Sn(O_2CR')_2$ has numerous representatives,[39] e.g. R = R′ = Me.[37] Water first coordinates to tin, represented by $Bu_2Sn(O_2CCH_2C_6H_5)_2(OH_2)$,[42] then the carbonyl groups free themselves from coordination to tin **(8)** allowing H^+ transfer from water, liberating $R'CO_2H$ and generating the hydroxy-carboxylate $R_2Sn(OH)(O_2CR')$, which dimerizes, as in the structure of $[^tBu_2Sn(OH)(O_2CMe)]_2$;[46] condensation then affords the dimeric stannoxane, typified by $\{[Me_2Sn(O_2CCCl_3)]_2O\}_2$.[47]

Gas-phase electron diffraction study of $Me_3SnO_2CC_2F_5$ (9)

Using the SARACEN method[34,35] to restrain 15 geometrical and 10 amplitude parameters, all 28 geometrical parameters were refined. The parameters are listed in Table 5, relating to the atom numbering shown in Fig. 1. Amplitudes of vibration for the most significant atom pairs are listed in Table 6, and

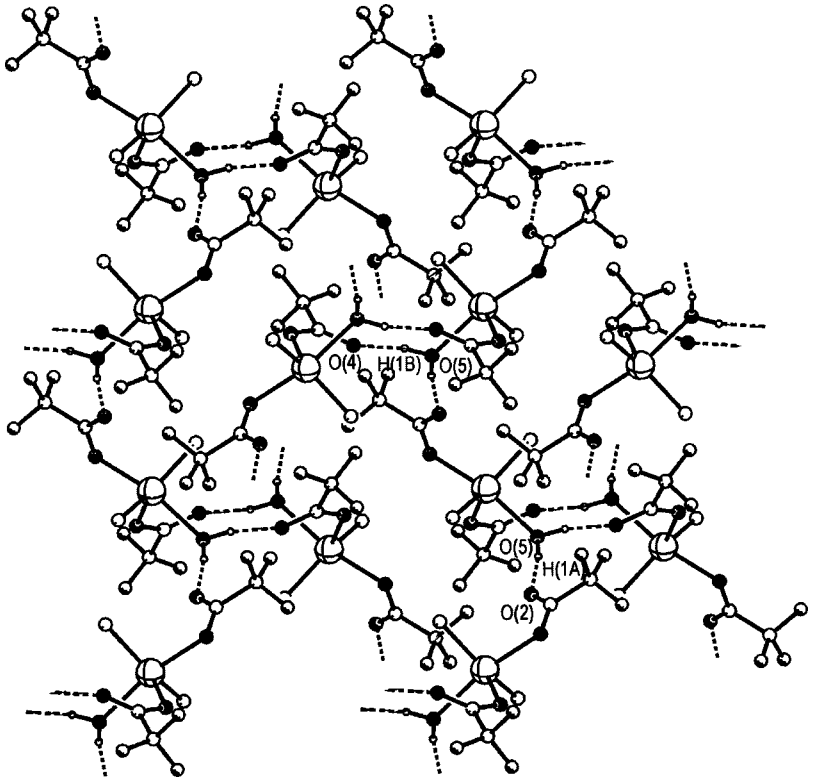

Figure 4. The lattice structure of **8** (viewed along [001]) showing the hydrogen bonding interactions.

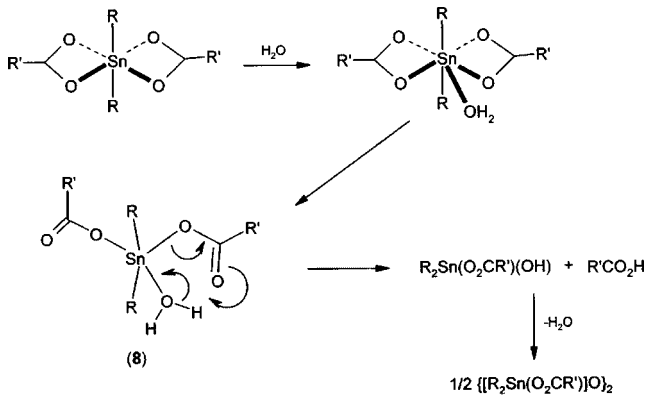

Scheme 1.

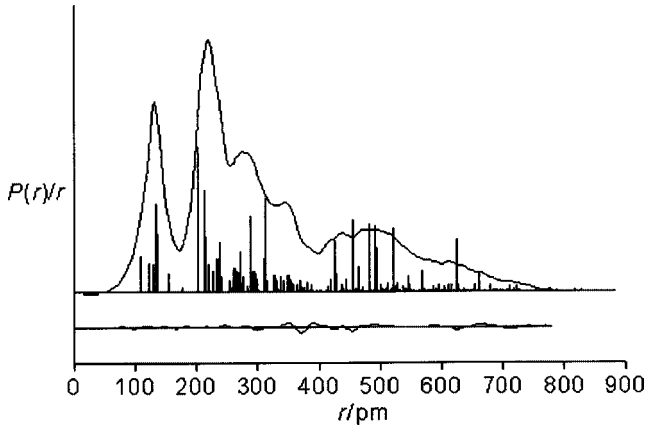

Figure 5. Experimental and difference (experimental minus theoretical) radial-distribution curves, $P(r)/r$, for $Me_3SnO_2CC_2F_5$. Before Fourier inversion the data were multiplied by $s\ \exp(-0.000\,02s^2)/(Z_{Sn} - f_{Sn})(Z_F - f_F)$.

a longer list is given in the supplementary Table S2. The final R factors were $R_G = 0.069$ and $R_D = 0.075$. The radial distribution curve and molecular scattering intensity curves are shown in Figs 5 and 6 respectively, and the least-squares correlation matrix is given in supplementary Table S3.

Neither the experimental data nor the *ab initio* calculations gave any evidence for a conformer in which a fluorine atom came close enough to the tin atom to interact with it significantly. Calculations showed there to be very little difference in most parameters for the two conformers, with the largest difference in bond length being observed for the C(5)–F(14) bond, which was 0.9 pm longer in conformer 2 (135.0 pm compared with 134.1 pm in conformer 1). Bond angles were also very similar in the two conformers.

Changes in the theoretical treatment resulted in some significant variations in geometrical parameters. The average Sn–C bond length changed the most on switching from the D95 basis set to the LanL2DZ pseudo-potential, with

Table 5. Refined and calculated geometric parameters for $Me_3SnO_2CC_2F_5$ (**9**) in the gas phase (distances in picometres, angles in degrees) from the GED study[a,b]

No.	Parameter	GED (r_a)	MP2/6-31G*	Restraint
p_1	Average C–H	109.8(1)	109.8	109.8(1)
p_2	Average Sn–C	214.1(3)	212.6	
p_3	Average C–C	153.7(5)	154.5	
p_4	Average C–F	134.5(2)	135.0	
p_5	[Average C(4)–F(10/11)] − [Average C(5)–F(12/13/14)]	1.6(1)	1.7	1.7(1)
p_6	Sn–O	201.6(10)	205.1	205.1(44)
p_7	C–O	129.2(13)	131.5	131.5(20)
p_8	C═O	122.7(7)	123.1	123.1(20)
p_9	Average C(4)–C(5)–F(12/13/14)	111.4(4)	110.3	
p_{10}	F–C–F	108.3(5)	108.3	108.3(5)
p_{11}	C(3)–C(4)–C(5) in conformer 1	114.5(5)	114.5	114.5(5)
p_{12}	O(2)–C(3)–C(4)	111.4(5)	111.6	111.6(5)
p_{13}	O(9)═C(3)–C(4)	121.1(6)	121.8	121.8(7)
p_{14}	O(2)–Sn(1)–C(6)	98.1(13)	98.1	98.1(142)
p_{15}	Average C(6)–Sn(1)–C(7/8)	117.3(15)	116.7	116.7(15)
p_{16}	Sn(1)–O(2)–C(3)	119.0(14)	114.2	114.2(50)
p_{17}	Average Sn–C–H	110.5(3)	110.6	110.6(3)
p_{18}	Average O(2)–Sn(1)–C(7/8)	105.6(5)	105.5	105.5(5)
p_{19}	C(3)–C(4)–C(5) in conformer 2	111.5(9)	112.8	112.8(10)
p_{20}	C(3)–C(4)–C(5)–F(12) in conformer 1	0.0	0.0	
p_{21}	C(3)–C(4)–C(5)–F(12) in conformer 2	18.4(19)	11.8	
p_{22}	O(2)–C(3)–C(4)–C(5) in conformer 1	180.0	180.0	
p_{23}	O(2)–C(3)–C(4)–C(5) in conformer 2	71.5(31)	63.2	
p_{24}	Sn(1)–O(2)–C(3)–C(4) in conformer 1	180.0	180.0	
p_{25}	Sn(1)–O(2)–C(3)–C(4) in conformer 2	−171.6(29)	−179.0	
p_{26}	Me_3 twist in conformer 1	0.1(9)	0.0	
p_{27}	Me_3 twist in conformer 2	−16.4(73)	1.4	
p_{28}	Weight of conformer 1	0.24	0.36	

[a] Figures in parentheses are the estimated standard deviations of the last digits.
[b] Unless stated otherwise, parameter definitions apply to both conformers.

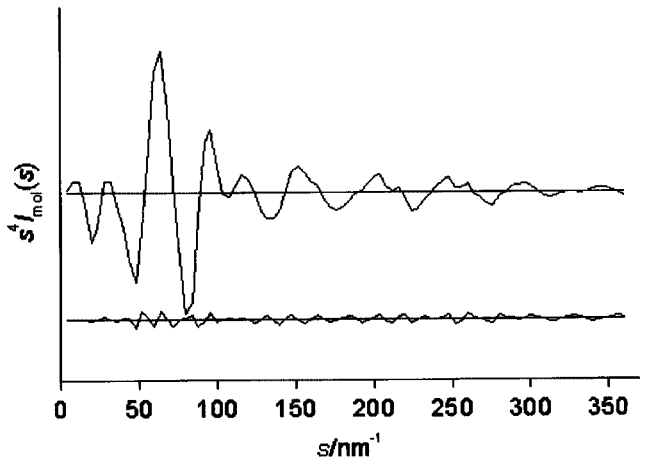

Figure 6. Combined experimental and final weighted difference (experimental minus theoretical) molecular-scattering intensities for $Me_3SnO_2CC_2F_5$.

a decrease in bond length of around 2 pm (~214.7 pm to ~212.6 pm). The unrestrained GED value for the average Sn–C bond was 214.1(3) pm, which is longer than calculated at the MP2 level by 1.5 pm. The Sn–O bond lengths also varied substantially with the theoretical treatment. At the D95/HF level it was calculated as 205.5 pm for the major conformer. It then shortened by around 5 pm with the switch to the LanL2DZ basis set on tin and finally lengthened by around 4.7 pm on moving to the MP2 level. The GED value of 201.6(10) pm suggests that the MP2 level of theory overestimates the length of the Sn–O bond (at least using this basis set). The C–C bond lengths were largely unaffected by changes in basis set and level of theory, and the average distance computed at the MP2 level (154.5 pm) falls within two standard deviations of the unrestrained GED value of 153.7(5) pm. C–F bonds lengthened by about 3 pm with the inclusion of electron correlation (at the MP2 level). C(4)–F(10/11) was found to be longer than C(5)–F(12/13/14) by about 1.5 pm. The C–O bond is not particularly sensitive

Table 6. Interatomic distances (r_a/pm) and amplitudes of vibration (u/pm) for the restrained GED structure of $Me_3SnO_2CC_2F_5$.[a] Only the most significant contributions to the molecular scattering intensity are listed

No.	Atom pair	Conformer	r_a/pm	u/pm[b]		Restraint
u_1	H(18)–C(6)	1 and 2	109.8	7.7	(fixed)	
u_3	O(9)–C(3)	1 and 2	122.8	3.7(4)		3.7(3)
u_5	C(3)–O(2)	1 and 2	129.2	4.2	(tied to u_3)	
u_7	F(12/13/14)–C(5)	1 and 2	133.7	4.8(3)		4.3(4)
u_9	F(10/11)–C(4)	1 and 2	135.3	4.8	(tied to u_7)	
u_{11}	C(4)–C(5)	1 and 2	153.7	5.0	(fixed)	
u_{12}	C(3)–C(4)	1 and 2	153.7	5.1	(fixed)	
u_{17}	O(2)–Sn(1)	1 and 2	201.6	5.9(6)		5.7(6)
u_{19}	C(6/7/8)–Sn(1)	1 and 2	214.1	4.6(4)		
u_{31}	O(2)···O(9)	1 and 2	226.0	4.9/5.0	(tied to u_{39})	
u_{33}	C(4)···O(3)	1 and 2	234.1	6.9	(tied to u_{39})	
u_{35}	F(10/11)···C(5)	1 and 2	234.8	6.9	(tied to u_{39})	
u_{36}	F(10/11)···C(3)	1	234.8	6.9	(tied to u_{39})	
u_{38}	F(10/11)···C(7)	2	237.0	6.9	(tied to u_{39})	
u_{39}	F(12/13/14)···C(4)	1 and 2	237.7	6.7(4)/6.9		6.9(7)
u_{65}	C(3)···Sn(1)	1 and 2	287.4	6.8(7)/7.3		6.7(7)
u_{76}	O(9)···Sn(1)	1 and 2	311.7	11.3(10)/12.3		10.6(11)
u_{187}	C(4)···Sn(1)	2	426.2	8.2	(tied to u_{217})	
u_{209}	F(10)···Sn(1)	2	455.8	12.6	(tied to u_{217})	
u_{217}	F(10/11)···Sn(1)	1	464.0	12.6(12)		11.9(12)
u_{234}	F(11)···Sn(1)	2	482.6	19.7	(tied to u_{217})	
u_{259}	C(5)···Sn(1)	2	493.0	11.6	(tied to u_{217})	
u_{283}	F(13/14)···Sn(1)	2	522.0	13.3	(tied to u_{317})	
u_{309}	C(5)···Sn(1)	1	545.7	7.7	(tied to u_{317})	
u_{317}	F(13/14)···Sn(1)	1	567.6	14.3(14)		14.1(14)

[a] Estimated standard deviations, obtained in the least-squares refinement, are given in parentheses.
[b] Amplitudes not refined were fixed at the values obtained using the HF/LanL2DZ-D95 force field.

to the addition of the pseudo-potential but does lengthen by ~3 pm from 128.3 pm at the D95/HF level to 131.5 pm at the MP2 level. The GED value of 129.2(13) lies somewhere between those given by the HF and MP2 levels of theory. Similarly, the C═O bond lengthens by ~4 pm from 119.5 pm at the D95/HF level to 123.3 pm at the MP2 level. The experimental GED value of 122.7(7) pm is close to that given by the MP2 level of theory.

The majority of bond angles varied little with changes in theoretical treatment. The exception to this is Sn(1)–O(2)–C(3). At the HF level, Sn(1)–O(2)–C(3) is found to be around 122°. At the MP2 level the angle is found to decrease by 8° to around 114.2°. However, the GED experimental value of 119.0(14)° does not support the small value calculated at the MP2 level. The angle O(2)–Sn(1)–C(6) is also interesting. At 98.1° (MP2) it is 4° smaller than the equivalent angle [C(2)–Sn(1)–C(6)] in $Me_3SnC_4F_9$ [13] and around 7.4° smaller than the angles O(2)–Sn(1)–C(7) and O(2)–Sn(1)–C(8). The GED value of 98.1(13)°, with an extremely weak restraint, confirms this particularly small angle, which can be attributed to the additional coordination of O(9) to tin, with the Sn···O distance being only 312 pm; O(9) approaches tin approximately trans to C(6) [<O(9)–Sn(1)–C(6): 146.8°]. The average C(6)–Sn(1)–C(7) and C(6)–Sn(1)–C(8) angles are found to be correspondingly larger than their counterparts in $Me_3SnC_4F_9$.[13] The existence of this non-bonded Sn···O interaction forces the C_2F_5 group to be directed away from the tin atom, and thus precludes any possibility of even a passing contact between a fluorine atom and tin. The situation is thus quite different from that pertaining in $Me_3SnC_4F_9$.[13] Here, it is only the third and fourth conformers that involves close Sn···F interactions, but their energy is such that at the temperature of the CVD experiments are present in sufficient abundance to account for the observed degree of fluorine doping of the deposited tin oxide. In the present case, the mechanism of fluorine transfer to tin would appear to be different.

CVD studies

Compounds tested were **1**–**3**, **6** and **7**. This selection allowed assessment of variations in the R groups (Bu, Et and Me), the length of the fluorinated chain (CF_3, C_2F_5 and C_3F_7), and the number of fluorine-containing ligands (one or

two). Although all of the triorganotin carboxylates form polymeric crystalline solids with melting points in the range 50–94 °C, good volatility was achieved with bubbler temperatures approximately 60 °C in excess of the melting points. The thermogravimetric analysis (TGA) of **9**, used in the GED study, shows that complete sublimation of the sample has taken place by *ca* 150 °C (Fig. 7). The diorganotin carboxylate **7** with a melting point of 140 °C only required a 25 °C increase in bubbler temperature in order to grow a suitable film. However, a higher temperature for the heater tapes was required for this precursor in order to prevent solidification in the pipework between bubbler and substrate.

Although the melting points of the ethyl- and methyltin compounds were higher than those of the butyltin compounds, the deposition durations for the former were markedly shorter than for the latter for the production of films of similar thickness. Films of *ca* 300 nm could be achieved within reasonable deposition times (Tables 1 and 7), and in the cases of **6** and **7**, which incorporate smaller hydrocarbon groups on tin, deposition times were reduced by an order of magnitude compared with those for the butyltin precursors. Films grown from the tributyltin carboxylates **1**–**3** were found to favour deposition at the front end of the substrate directly after the inlet, and only coated the first ca 5 cm of the glass.

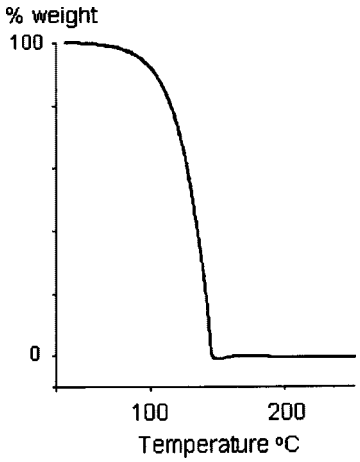

Figure 7. TGA of **9**.

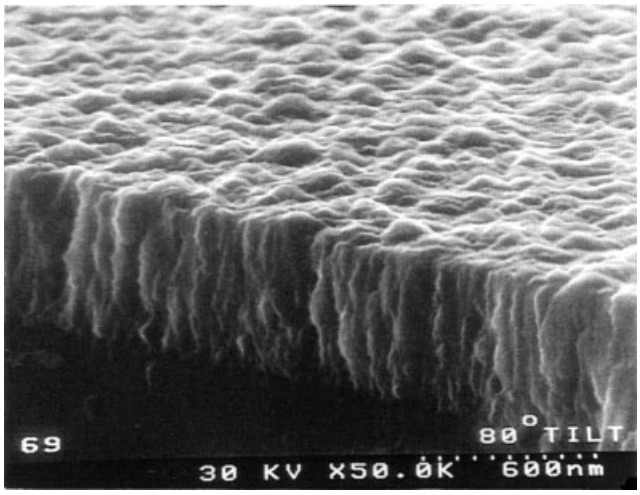

Figure 8. Scanning electron micrograph of the F : SnO_2 film deposited from precursor **2**.

Films derived from $Et_3SnO_2CC_2F_5$ (**6**) and $Me_2Sn(O_2CCF_3)_2$ (**7**) had a much more uniform appearance and the coating spanned the total length of the substrate. Scanning electron microscopy (SEM) was performed on the film deposited from $Bu_3SnO_2CC_2F_5$ (**2**) and revealed a uniform film with a smooth surface and homogeneous substrate coverage (Fig. 8).

All the films were crystalline, and glancing-angle X-ray diffraction confirmed the film composition as tin oxide in all cases (Table 8); a typical diffraction pattern is shown for the film grown from $Bu_3SnO_2CC_2F_5$ (**2**) in Fig. 9. It is known that for a random specimen of SnO_2, the (200) reflection should make up 7% of the spectral intensity and that films of SnO_2 grown preferentially along the (200) direction contain fewer structural defects than randomly oriented materials.[49,50] For all films deposited in this study the preferred orientations were shown by the more intense (110), (101), (200) and (211) peaks. The proportions found for the (200) reflection were very high for **1**–**3, 6** and were well in excess of 7%. In contrast, the contribution from the (200) reflection to the spectrum of the film from the diorganotin carboxylate (**7**) was very low at 4.2%, suggesting that the films grown from the triorganotin derivatives appeared to have greater

Table 7. Analysis of fluorine-doped SnO_2 films from fluorinated organotin carboxylate precursors

	1	**2**	**3**	**6**	7	Std[a]
Thickness (nm)	360.0	515.0	300.0	347.0	293.5	300
Haze (%)	0.56	0.99	0.59	0.39	0.28	<0.40
Emissivity	0.147	0.118	0.175	0.167	0.304	<0.150
Sheet resistance (Ω/□)	13	8	18	16	39	15
Resistivity ($\times 10^{-3}$ Ω cm)	0.46	0.43	0.54	0.54	1.13	0.50
Fluorine content (at.%)	1.02	1.02	0.88	1.16	4.80	2.00

[a] Typical measurements for a good fluorine-doped tin oxide film derived from separate tin and fluorine sources.[48]

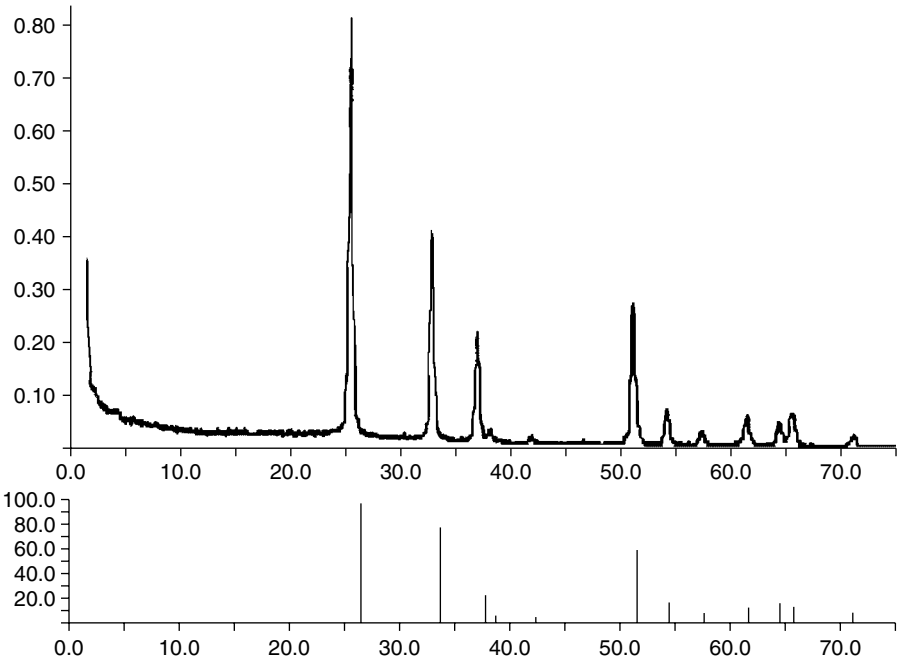

Figure 9. Powder XRD of the F : SnO_2 film deposited from precursor **2**. Below is shown the pattern for a randomly oriented samples of SnO_2 (cassiterite, PDF 21-1250).

structural integrity. From line broadening measurements of the (110) reflection it was possible to measure the approximate crystallite sizes of the samples, which lie in the range 15.1–32.0 nm.

Energy-dispersive X-ray analysis indicated fluorine was present in all the films, though X-ray fluorescence measurements showed that the amount of halogen remained approximately constant (*ca* 1%) across the series of $R_3SnO_2CR_f$ (**1–3, 6**), despite the increasing fluorine content of the R_f group (Table 7). This suggests both a common decomposition pathway for all the precursors and that delivery of fluorine from only one carbon centre is important. Given that there are no close Sn···F contacts in the gas-phase structures of the triorganotin fluorocarboxylates as evidenced by the GED study of **9**, direct transfer of halogen to tin is highly unlikely. The most plausible mechanism would involve loss of CO_2 to generate R_3SnR_f, which we have shown to be viable (if relatively difficult to synthesize) precursors for F:SnO_2 in their own right.[13] The electron impact mass spectrum of **9**, which gives some clues as to the mode of decomposition, has P–Me (*m/z* 313) as the major fragment (100%), along with minor fragments corresponding to Me_2Sn (*m/z* 150, 10%), MeSn (*m/z* 135, 25%) and Sn (*m/z* 120, 10%). In addition, there is a cluster of overlapping fragments with *m/z* 160–169 (80%), which probably includes Me_3Sn (*m/z* 165), but this alone does not account for the isotope distribution profile. The most abundant fragment in this cluster at *m/z* 169 could reasonably correspond to Me_2SnF, which would be arrived at by loss of CO_2 and C_2F_4 from $Me_2SnO_2CC_2F_5$.

The high fluorine content in the film derived from **7** at 560 °C (*ca* 4.8%) is surprising. $Bu_2Sn(O_2CCF_3)_2$ has been used to grow F:SnO_2 with fluorine contents of 0.5–1.5% at temperatures of 370–490 °C, and, while the amount of fluorine incorporated was seen to increase with increasing temperature, somewhat less than 4.8% that might have been anticipated had the decomposition been made at 70 °C

Table 8. XRD data for the fluorine-doped SnO_2 films deposited from organotin fluorocarboxylate precursors

(*hkl*)	Angle (°)	**1**	**2**	**3**	**6**	**7**
(110)	26.6	513	175	165	145	127
(101)	33.9	221	332	316	302	154
(200)	37.9	673	566	340	254	21
(111)	39.0	0	0	0	0	0
(210)	42.6	27	27	27	28	0
(211)	51.7	457	537	500	481	154
(220)	54.8	98	40	29	31	3
(002)	57.8	0	0	0	0	0
(310)	61.9	109	122	85	75	19
(112)	64.7	0	27	0	0	0
(301)	66.0	82	66	37	28	9
Total counts		2180	1893	1499	1344	488
(200) (total as percentage)		30.9	29.9	22.7	18.9	4.2
Crystallite size nm		32.0	19.3	18.3	15.1	—[a]

[a] Could not be calculated.

higher.[4] This suggests that the decomposition pathway is different to that of **7**, possibly by virtue of the absence of β - hydrogen atoms on the hydrocarbon groups of the latter. Butyl groups attached to tin can undergo butene elimination generating Sn–H bonds, which then offer the possibility of HF elimination (by a radical mechanism involving $H^{\cdot}$), a sequence that cannot be replicated by methyl tin precursors. Interestingly in this respect, inorganic tin precursors such as $Sn(O_2CCF_3)_2$ and $Sn[OCH(CF_3)_2]_4(HNMe_2)_2$ also generate more highly doped F:SnO_2 films (*ca* 2.5%).[1,2]

Film properties

The physical properties of the films are given in Table 7 and compared with those for films generated by a commercial dual-source approach.[48] All of the films generated have a thickness typical of those used in solar control coatings, and those derived from **6** and **7** have comparable levels of haze (<0.40%); films derived from **1**–**3**, however, are less visually clear (haze 0.59–0.99%). The films generated by **1**–**3** and **6** all have emissivity (0.118–0.175), sheet resistance (8–16 Ω/□) and resistivity ($0.43–0.54 \times 10^{-3}$ Ω cm) that compare favourably with a commercial product, despite the fact that in none of the deposition experiments have the experimental conditions been optimized. In contrast, the properties of the film produced by **7** are notably inferior to those of both the commercial sample and of the above experimental films. The nature of the fluorine doping seems to be crucial, as the dopant level from **7** is by far the highest. The deterioration of film properties and the reduced (200) preferred orientation suggest that at least some of the fluorine is not necessarily integral to the SnO_2 lattice.

CONCLUSIONS

Fluorine-doped SnO_2 films with properties approaching those of commercial products can be achieved using the organotin fluorocarboxylates $R_3SnO_2CR_f$. The fastest growth rates are achieved from Et_3Sn (rather than Bu_3Sn) derivatives. The fluorine content of all the films is *ca* 1%. In particular, $Et_3SnO_2CC_2F_5$ gives excellent films, with rapid growth rates, and is a viable atmospheric pressure CVD precursor, despite adopting a polymeric structure in the solid state. Films grown from $Me_2Sn(O_2CCF_3)_2$ contain higher levels of fluorine dopant but exhibit diminished physical properties. The gas-phase structure of $Me_3SnO_2CC_2F_5$ indicates that accessible conformations do not allow contact between tin and fluorine, and that direct transfer, therefore, is unlikely to be part of the mechanism for fluorine incorporation in SnO_2 films. A mechanism that involves loss of CO_2 to generate R_3SnR_f *in situ* seems likely.

Acknowledgements

We acknowledge support from Pilkington plc (for J.E.S.), EPSRC (for J.E.S., B.F.G., and the gas electron diffraction service; GR/R17768). We thank Mr J. Lewis (Institute of Astronomy, Cambridge) for tracing photographic plates and Dr S. L. Hinchley for helpful discussions.

REFERENCES

1. Maruyama T, Tabata K. *J. Appl. Phys.* 1990; **68**: 4282.
2. Suh S, Hoffman DM, Atagi LM, Smith DS, Liu J-R, Chu W-K. *Chem. Mater.* 1997; **9**: 730.
3. Suh S, Hoffman DM. *Inorg. Chem.* 1996; **35**: 6164.
4. Suh S, Zhang Z, Chu W-K, Hoffman DM. *Thin Solid Films* 1999; **345**: 240.
5. Stanley JE. The synthesis of single-source precursors for the CVD of F-doped tin oxide. PhD thesis, University of Bath, 1997.
6. Elich JJP, Boslooper EC, Haitjema H. *Thin Solid Films* 1989; **177**: 17.
7. Price LS, Parkin IP, Field MN, Hardy AME, Clark RJH, Hibbert TG, Molloy KC. *J. Mater. Chem.* 2000; **10**: 527.
8. Menke AG. *German Patent* 2246193; *Chem. Abstr.* 1973; **78**: 150 521.
9. Bloss KH, Davis JA, Neuman GA, Harmon PP. *European Patent* 338 417; *Chem. Abstr.* 1989; **112**: 82 817.
10. Durant M, Merienne G, Valette D. *European Patent* 623 564; *Chem. Abstr.* 1994; **122**: 62 398.
11. Kemmer M, Dalil H, Biesemans M, Martins JC, Mahieu B, Horn E, de Vos D, Tiekink ERT, Willem R, Gielen M. *J. Organometal. Chem.* 2000; **608**: 63.
12. Molloy KC, Purcell TG, Quill K, Nowell I. *J. Organometal. Chem.* 1984; **267**: 237.
13. Stanley JE, Swain AC, Molloy KC, Rankin DWH, Robertson HE, Johnston BF. *J. Appl. Organometal. Chem.* 2004; In press.
14. Edwards DA, Harker RM, Mahon MF, Molloy KC. *J. Mater. Chem.* 1999; **9**: 1771.
15. Kaelble EF. *Handbook of X-Rays*. McGraw-Hill: New York, 1967; chapter 17.
16. Bass M. *Handbook of Optics*, 2nd edition. McGraw Hill: New York, 1995.
17. Zuckerman JJ, Debye NW, Fenton DE, Ulrich SE. *J. Organometal. Chem.* 1971; **28**: 339.
18. Laliberte BR, Reiff HF, Davisdsohn WE. *Org. Prep. Proc.* 1969; **1**: 173.
19. Anderson HH. *Inorg. Chem.* 1962; **1**: 647.
20. Sheldrick GM. SHELX 86S, a computer program for crystal structure determination. University of Göttingen, Göttingen, 1986.
21. Sheldrick GM. SHELX 93, a computer program for crystal structure refinement. University of Göttingen, Göttingen, 1993.
22. McArdle P. *J. Appl. Crystallogr.* 1995; **28**: 65.
23. Walker N, Stewart D. *Acta Crystallogr. Sect. A: Found. Crystallogr.* 1983; **39**: 158.
24. Frisch MJ, Trucks GW, Schlegel HB, Gill PMW, Johnson BG, Robb MA, Cheesman JR, Keith TA, Petersson GA, Montgomery JA, Raghavachari K, Al-Laham MA, Zakrzewski VG, Ortiz JV, Foresman JB, Cioslowski J, Stefanov BB, Nanayakkara A, Challacombe M, Peng CY, Ayala PY, Chen W, Wong MW, Andres JL, Replogle ES, Gomperts R, Martin RL, Fox DJ, Binkley JS, Defrees DJ, Baker J, Stewart JP, Head-Gordon M, Gonzalez C, Pople JA. Gaussian 94 (Revision C.2). Gaussian Inc., Pittsburgh, PA, 1995.
25. Dunning THJ, Hay PJ. In *Modern Theoretical Chemistry*. Ed. Schaefer I HF (ed.). Plenum: New York, 1976; 1.
26. Hay PJ, Wadt WR. *J. Chem. Phys.* 1985; **82**: 270.
27. Wadt WR, Hay PJ. *J. Chem. Phys.* 1985; **82**: 284.
28. Hay PJ, Wadt WR. *J. Chem. Phys.* 1985; **82**: 299.
29. Hedberg L, Mills IM. *J. Mol. Spectrosc.* 1993; **160**: 117.
30. Scott AP, Radom L. *J. Phys. Chem.* 1996; **100**: 16 502.

31. Huntley CM, Laurenson GS, Rankin DWH. *J. Chem. Soc. Dalton Trans.* 1980; 954.
32. Hinchley SL, Robertson HE, Borisenko KB, Turne AR, Johnson BF, Rankin DWA, Ahmadlan M, Jones JN, Lowley AH. *J. Chem. Soc. Dalton Trans.* 2004; 2469.
33. Ross AW, Fink M, Hilderbrand R. In *International Tables for Crystallography*, Wilson AJC (ed.). Kluwer: Dordrecht, 1992; 245.
34. Blake AJ, Brain PT, McNab H, Miller J, Morrison CA, Parsons S, Rankin DWH, Robertson HE, Smart BA. *J. Chem. Phys.* 1996; **100**: 12 280.
35. Brain PT, Morrison CA, Parsons S, Rankin DWH. *J. Chem. Soc. Dalton Trans.* 1996; 4589.
36. Uesugi H, Kawai S, Inaba T. *Chem. Abstr.* 1970; 90 636.
37. Lockhart TP, Davidson F. *Organometallics* 1987; **6**: 2471.
38. Davies AG, Smith PJ. Tin. In *Comprehensive Organometallic Chemistry*, Wilkinson G, Stone FGA, Abel EW (eds). Pergamon Press: Oxford, 1982; 519.
39. Lockhart TP, Manders WF. *Inorg. Chem.* 1986; **25**: 892.
40. Tiekink ERT. *Trends Organometal. Chem.* 1994; **1**: 71.
41. Misty F, Rettig SJ, Trotter J, Aubke F. *Z. Anorg. Allg. Chem.* 1995; **621**: 1875.
42. Ng SW, Chen W, Zainudin A, Kumar Das VG, Yip W-H, Wang R-J, Mak TCW. *J. Crystallogr. Spectrosc. Res.* 1991; **21**: 39.
43. Dakternieks D, Kuan FS, Tiekink ERT. *Main Group Met. Chem.* 2001; **24**: 291.
44. Sang X, Yang Z, Xie Q, Li J, Xueqing S, Zhiqiang Y, Qingla X, Jinshan L. *J. Organometal. Chem.* 1998; **566**: 103.
45. Davies AG. *Organotin Chemistry*. Verlag Chimie: Weinhein, 1997; 144.
46. Mokal VB, Jain VK, Tiekink ERT. *J. Organometal. Chem.* 1992; **431**: 283.
47. Alcock NW, Roe SM. *J. Chem. Soc. Dalton Trans.* 1989; 1589.
48. Soubeyrand MJ, Halliwell AC. *US Patent* 5 698 262, 1997.
49. Bélanger D, Dodelet JP, Lombos BA, Dickson JI. *J. Electrochem. Soc.* 1985; **132**: 1398.
50. Smith A, Laurent J-M, Smith DS, Bonnet J-P, Clemente RR. *Thin Solid Films* 1995; **266**: 20.

